01,02,05

Ab initio calculation of the band structure and properties of modifications of the Ti_3Sb compound doped with lithium

© M.M. Asadov[1,2], S.O. Mammadova[3], S.S. Guseinova[3], S.N. Mustafaeva[3], V.F. Lukichev[4]

[1] Nagiyev Institute of Catalysis and Inorganic Chemistry, Azerbaijan National Academy of Sciences, Baku, Azerbaijan
[2] Scientific Research Institute Geotechnological Issues Problems of Oil, Gas and Chemistry of Azerbaijan State University Oil and Industry, Baku, Azerbaijan
[3] Institute of Physics, Azerbaijan National Academy of Sciences, Baku, Azerbaijan
[4] Valiev Institute of Physics and Technology, Russian Academy of Sciences, Moscow, Russia

E-mail: mirasadov@gmail.com

Received July 2, 2022
Revised July 2, 2022
Accepted July 3, 2022

Using the density functional theory (DFT) in the local electron spin density approximation (LSDA), $2 \times 2 \times 2$ supercells based on the Ti_3Sb compound have been studied. The supercells contained their own vacancies and doped lithium atoms replacing Ti and/or Sb. The DFT-LSDA method was used to calculate the structural, electronic, and magnetic properties, the enthalpy of formation, and the cohesion energy of supercells of two modifications of the Ti_3Sb compound. We studied supercells with cubic system (A15 type structure; $a = 5.217$ Å) and tetragonal system ($D8_m$ type structure; $a = 10.457$ Å, $c = 5.258$ Å). It has been established that the distribution of the density of states of the Ti_3Sb cubic system has a more metallic character than for the $D8_m$ Ti_3Sb modification. The enhancement of „metallicity" in the cubic modification A15 Ti_3Sb is associated with an increase in the Ti−Sb interatomic distance in the crystal. Due to this, the degree of metallic bonding increases during the electronic interaction between Ti and Sb atoms near the Fermi level in Ti_3Sb.

In DFT calculations, the spin-polarized density of states was taken into account. It has been established that in both modifications (A15 and $D8_m$) of Ti_3Sb near the Fermi level for *s*-, *p*-, *d*-states with spin „up" and spin „down" there is a spin imbalance in the population of energy levels.

Defect-containing supercells based on Ti_3Sb were studied by DFT-LSDA calculations. It is shown that Ti and/or Sb vacancies in the lattices of Ti_3Sb crystals of both modifications (A15 and $D8_m$) increase the magnetic moment (M) as compared to the value of M ($M = 0.08\,\mu_B$) of a „pure" Ti_3Sb crystal. Considering that Al5 Ti_3Sb is also interesting as a material for Li-ion batteries, we studied Ti_3Sb−Li supercells doped with lithium. Li-doping and the creation of own Ti and/or Sb vacancies changes the distance between atoms in Ti_3Sb. Correspondingly, the resulting local magnetic moments near the Ti or Sb vacancies also change. The enthalpy of formation and magnetic moment of Ti_3Sb and Ti_3Sb−Li based supercells are calculated. DFT calculations of the structural stability of binary compounds (phases) have been carried out, and the stability of conodes between phases in the Ti−Sb−Li system has been established. The isothermal section of the Ti−Sb−Li system was plotted at 298 K. It is shown that the introduction of various lithium concentrations (≤ 6.25 at.% Li) into the Ti_3Sb (Space group $Pm\bar{3}n$; № 223; $a = 5.217$ Å) crystal lattice reduces the partial magnetic moment of Ti in the Ti_3Sb−Li supercell.

Keywords: Ti_3Sb intermetallic compounds, A15 cubic modification, $D8_m$ tetragonal modification, doping with lithium, Ti_3Sb−Li, DFT-LSDA calculations, supercell, electronic and magnetic properties, Ti−Sb−Li phase stability.

DOI: 10.21883/PSS.2022.11.54179.395

1. Introduction

Intermetallic compounds (intermetallides) are used as a basis in industrial alloys. Due to this, fundamental studies of the peculiarities of structural-phase states in binary intermetallides are important. This is required in the development of structural and physical basics for the development of alloys having the specified properties. Intermetallides of binary compounds of stoichiometric ratios are known, in particular, AB and A_3B. A_3B alloys contain intermetallides of the cubic, tetragonal and hexagonal crystal system. A class of intermetallides of transition metals with the A15 structure and A_3B stoichiometry, which manifest superconducting properties with high critical parameters, is known [1]. Due to this, much attention is paid to the study of A_3B intermetallides with the A15 structure. The properties of A15 alloys are conditioned by their crystal structure, while the presence of high-temperature superconductivity is related to structural instability. Thereat, the electronic band structure of compounds with A15 phases reflects

the quasi-one-dimensional nature of chains of A atoms. The study of electronic properties of Ti_3Sb, Ti_3Ir [2], Ta_3Sb, Ta_3Pb and Ta_3Sn [3] compounds with a cubic crystal system (phase A15, prototype Cr_3Si) indicates their superconductivity. The band structure of A15 compounds with a spin-orbit coupling is characterized by an energy gap near the Fermi level. A_3B intermetallic phase have the superconductivity temperature $T_c = 5-20\,K$ (for Ti_3Sb $T_c = 6.7\,K$).

Intermediate phases based on binary systems, in particular, Ti–Sb [4–13] also have other areas of practical application. Alloys containing titanium antimonides are used as electrode materials for lithium batteries, e.g., TiSnSb alloys [14–20].

Considering the aforesaid, the study of ternary intermetallic phases in Ti–Sb–Me systems is of current interest. Only separate alloys were studied in these systems and several new compounds were found [21–32]: Ti–Sb–Fe [21,22], Ti–Sb–Si [23], Ti–Sb–X [24], Ti–Sb–Mn [25], Ti–Sb–Sn [26], Ti–Sb–Ni [27,28], Ti–Sb–Ce(Gd) [29], Ti–Sb–V (Cr, Mn, Fe, Co, Ni) [30], Ti–Sb–RE [31], Ti–Sb–(Si, Ge) [32], Ti–Sb–Ni [33]. Their crystal structure, magnetic and transport properties were studied.

However, phase interactions in the Ti–Sb–Li ternary system have not been studied up to the present. Phase diagrams of boundary binary systems Ti–Sb [4–6], Ti–Li [34], Sb–Li [35–39] and properties of binary compounds (in particular, Ti_3Sb, Ti_5Sb_3, $Ti_{11-x}Sb_{8-y}$, TiSb, Ti_5Sb_8, $TiSb_2$ [6], Li_3Sb, Li_2Sb [35–39]) of the Ti–Sb–Li ternary system have been studied experimentally.

Ti–Sb. According to [4], four titanium antimonides exist in the Ti–Sb system: Ti_3Sb (cubic crystal system Cr_3Si-type) and Ti_5Sb_3 (tetragonal crystal system W_5Si_3-type [5]), two compounds with rhombic structure $Ti_{1.7}Sb$ (space groups $Pmma$, $Pmc2_1$ or $Pma2$) and $Ti_{1.2}Sb$ ($Pbam$ or $Pba2$). The authors of [5] showed that the Ti_3Sb cubic phase irreversibly transforms into a tetragonal modification due to structure stabilization by aluminum and silicon impurities.

A revised phase diagram of the Ti–Sb system is given in paper [6] which describes the discovered binary compounds Ti_3Sb (melts incongruently at 1375°C; has a homogeneity range of 21.9–24.4 at.% Sb), Ti_2Sb (melts incongruently at 1422°C), Ti_5Sb_3 (melts incongruently at 1600°C), $Ti_{11-x}Sb_{8-y}$ (melts incongruently at 1328°C; has a homogeneity range of 41.9–43 at.% Sb), TiSb (melts incongruently at 1252°C; has a homogeneity range of 49.5–50 at.% Sb), Ti_5Sb_8 (melts incongruently at 1092°C; has a homogeneity range of 0.3 at.%; exists in the temperature range of 950–1092°C), $TiSb_2$ (melts incongruently at 1051°C). Restricted regions of solid solutions ($\sim$ 8–10 at.% Sb) form on the basis of the α–Ti and β–Ti modifications. The crystallographic data for the binary phases, pertaining to the Ti–Sb system, is also given there.

Ti–Li. Paper [34] describes the phase diagram of a Li–Ti boundary system where binary compounds and solid solutions do not form. Up to the temperature of 181°C, alloys of the Li–Ti system consist of a mixture of modifications of the initial components α-Li + β–Ti.

Li–Sb. The boundary Li–Sb binary system [35–39] has also been studied experimentally. Paper [35] gives the phase diagram of the Li–Sb system, showing the formation of two binary compounds: Li_3Sb (melts congruently at 1150°C) and Li_2Sb (melts incongruently at 585°C). Papers [38,39] give the results of thermodynamic studies of alloys and compounds of the Li–Sb system.

The stability of crystal structures of metal systems and their compounds is determined by two energy components: electrostatic contribution of ions and band contribution of valence electron energy. The ratio of atomic sizes in intermetallides is also important for the formation of different modifications. It is known that electrostatic contribution to the crystal lattice energy, in particular, of binary intermetallides depends on atomic volume as $\Omega^{-1/3}$, while the band contribution of valence electron energy depends on atomic volume as $\Omega^{-2/3}$. It means that the formation of different modifications of intermetallic phases also depends on the said energy contributions. Given the above-mentioned reasons, it is interesting to use ab initio calculations to determine the band structure of Ti_3Sb compounds with impurities.

The aim of the present paper is an ab initio calculation of electronic, magnetic properties and phase stability of supercells based on Ti_3Sb intermetallic phases with a cubic (type A15) and tetragonal crystal system (type $D8_m$ Ti_3Sb), containing lithium and/or vacancies.

2. Model and calculation procedure

Electronic and magnetic properties of two modifications of the Ti_3Sb compound doped with lithium Ti_3Sb–Li (cubic crystal system of type A15 Ti_3Sb and tetragonal crystal system of type $D8_m$ Ti_3Sb) were calculated under the density functional theory (DFT). Densities of states (DOS) for the given compound were also calculated. Calculations were performed using the Atomistix ToolKit software at $T = 0\,K$. Exchange-correlation functional E_{XC} was calculated in the local spin density approximation (LSDA) in the Perdew–Zunger parameterization [40–42]. The basis of linearized Muffin–Tin (MT) orbitals included Ti — [Ar] $3d^2 4s^2$-states of titanium, Sb — [Kr] $4d^{10} 5s^2 5p^3$-states of antimony and Li $1s^2 2s^1$. The structure of the Ti_3Sb crystal was used as a basis to make a supercell sized $2 \times 2 \times 2$ of the unit cell, where the given positions were occupied by Ti, Sb and Li atoms. Integration in reciprocal space was performed according to the Monkhorst–Pack scheme with a grid of $2 \times 2 \times 2$ k-points in the Brillouin zone.

Table 1. Crystallographic data for binary compounds of the Ti–Sb system

Compound	Type of structure	Space group	Cell parameters, Å			Reference
			a	*b*	*c*	
Ti_3Sb	Cr_3Si	$Pm\bar{3}n$	5.2228			11
Ti_3Sb	Cr_5Si_3	$I4/mcm$	10.465		5.2639	5
Ti_2Sb	Ti_2Sb	$I4/mmm$	3.9546		14.611	13
Ti_5Sb_3	Yb_5Sb_3	$Pnma$	10.2182	8.3432	7.1748	22
$Ti_{4.8}Sb_{3.3}$	Ti_5Ga_4	$P6_3/mcm$	7.982		5.515	12
$Ti_{10.84}Sb_{7.73}$	$Cr_{11}Ge_8$	$Pnma$	14.6228	5.5972	17.644	7
TiSb	NiAs	$P6_3/mcm$	4.123		6.265	24
Ti_5Sb_8	$Zr_{2.6}Ti_{2.4}Sb_8$	$I4_122$	6.492		26.514	31
$TiSb_2$	$CuAl_2$	$I4/mcm$	6.660		5.818	8
Ti	Mg	$P6_3/mcm$	2.9511		4.6843	9
Sb	As	$R\bar{3}m$	4.3084		11.247	9

Kinetic cutoff energy in the calculations was 150 Ry. A unit cell of Ti_3Sb was relaxed and optimized with the force and voltage tolerances of 0.01 eV/Å and 0.01 eV/Å^3 respectively. The DFT-LSDA calculations of Ti_3Sb–Li electronic properties used 64 atom $2 \times 2 \times 2$ supercells based on the Ti_3Sb compound, which contained vacancies and doped lithium atoms which substituted Ti and/or Sb. We have performed comparative calculations of the atomic magnetic moment based on Ti_3Sb $2 \times 2 \times 2$ supercells with the subsequent substitution of one or several Ti and/or Sb atoms by Li atoms. Lattice parameters were selected based on the condition of the minimum energy per one unit cell by the relaxation of interatomic distances inside the cell till the forces acting on the atoms are equal to zero.

3. Results and discussion

As mentioned above, the formation of seven binary compounds in the Ti–Sb system has been found: Ti_3Sb, Ti_2Sb, Ti_5Sb_3, $Ti_{11-x}Sb_{8-y}$, TiSb, Ti_5Sb_8, $TiSb_2$ [6]. The analysis of physical/chemical and structural data shows that the considered Ti_3Sb compound crystallizes in the form of two modifications: cubic (structural type A15, space group $Pm\bar{3}n$ $a = 5.2228$ Å [11]) and tetragonal crystal system (structural type $D8_m$, $I4/mcm$; $a = 10.465$ Å; $c = 5.2639$ Å [5]).

A polymorphic transformation A15 $\leftrightarrow D8_m$ to Ti_3Sb takes place with an increase of the system symmetry. Temperature of A15 $\leftrightarrow D8_m$ of a 2-nd order phase transition was not found during the differential thermal analysis of Ti–Sb alloys [6]. The incongruent melting temperature of the Ti_3Sb cubic modification is 1375°C. Therefore, A15 Ti_3Sb is also interesting from the viewpoint of high-temperature applications, e.g., as a material for Li-ion storage batteries. Moreover, A_3B intermetallic compounds with a cubic crystal system have a relatively high superconducting transition temperature.

3.1. Atomic and band structures: A15 Ti_3Sb (cubic crystal system)

3.1.1. Atomic structure

Positions A in the A15 structure of A_3B intermetallides are occupied by transition elements from groups IV, V, VI, while positions B are occupied both by transition and non-transition elements from group III. Compounds of type A15 have a primitive cubic unit cell of 8 atoms. Such an A_3B cell has two B atoms at positions (0, 0, 0) and (0.5, 0.5, 0.5) and six A atoms at positions (0, 0.5, 0.75), (0.5, 0.75, 0), (0, 0.5, 0.25), (0.5, 0.25, 0), (0.25, 0, 0.5) and (0.75, 0, 0.5).

The relaxed and optimized parameters of the cell, both of a cubic crystal system A15 Ti_3Sb (space group $Pm\bar{3}n$; № 223) with the lattice parameter $a = 5.217$ Å, $V = 141.99$ Å with the lattice parameter $a = 5.217$ Å, $V = 141.99$Å, and of a tetragonal crystal system $D8_m$ Ti_3Sb (space group $I4/mcm$; № 140), with the lattice parameters $a = 10.457$ Å, $c = 5.258$ Å, agree well with the experimental data (Table 1).

Fig. 1 shows the atomic structure of the cubic crystal system of A15 Ti_3Sb and the direction of local magnetic moment. In this structure, Ti atoms in Ti_3Sb form a system of three non-interacting orthogonal linear „chains“. Such „chains“ of Ti atoms are parallel to the edges of the Ti_3Sb unit cell. Superconducting properties of the A15 Ti_3Sb compound are, in particular, determined by such „chains„ of Ti atoms.

3.1.2. Electronic structure

The results of the DFT-LSDA calculations of the band structure of A15 Ti_3Sb at $T = 0$–300 K were identical along the directions of high symmetry. Fig. 2 shows the band structure of the cubic crystal system of the $2 \times 2 \times 2$ supercell of A15 Ti_3Sb, plotted for points of high symmetry of the R–X–M–G–P–X $2 \times 2 \times 2$ supercell. In the band structure of Ti_3Sb (Fig. 2, *a*) there are electron transitions from the valence band to the conduction band. Metallic

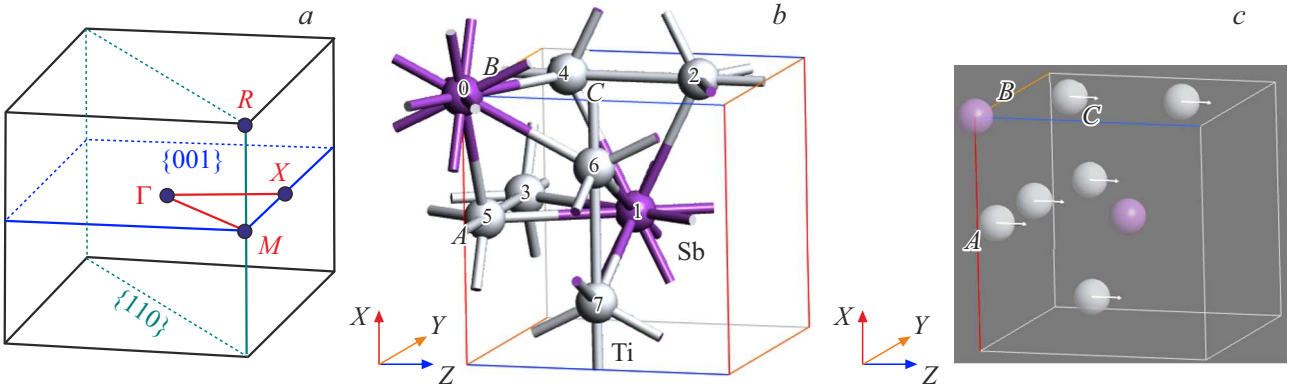

Figure 1. Structure of cubic crystal system of A15 Ti_3Sb compound (space group $Pm\bar{3}n$; № 223). *a*) Brillouin zone (BZ) for A15 (space group $Pm3n$), *b*) relaxed atomic structure of A15 Ti_3Sb, *c*) magnetic moment direction in the A15 Ti_3Sb supercell. Sb atoms are painted purple, while Ti atoms are gray.

conduction in Ti_3Sb is mainly ensured by *d*-states of Ti. We did not take into account the Coulomb correction for *d*-states of Ti in the DFT calculations.

Modelling of exchange-correlation interactions (XC) is the main difficulty of the DFT-calculation. Single-particle self-consistent DFT-LSDA calculations of electron density $n(\vec{r})$ of states of $2 \times 2 \times 2$ supercells were performed with the consideration of a different number of wave vectors $(\vec{k})$. Coordinates of $\vec{k}$ were chosen with a constant increment on each of the three axes (x, y, z) of the first Brillouin zone (Fig. 1, *a*). DOS was plotted for each set of wave vectors. It is assumed in DFT-LDA calculations of exchange energy (model of homogeneous electron gas) that the value $n(\vec{r})$ of an atom, ion, molecule or solid body at each space point is the same. The value $n(\vec{r})$ determines the particle count $N = \int n(\vec{r})dr$ and external potential $V(\vec{r})$. Then the complete Hamiltonian H of the electronic system in an adiabatic approximation is

$$\hat{H} = T + U + \sum_{i=1}^{N} V(\vec{r}_i),$$

where $\vec{r}$ is the coordinate of the i-th electron, T is the operator of electron kinetic energy, U is electron electrostatic repulsion energy. In other words, by solving the Schredinger equation $\hat{H}\psi(\vec{r}) = E\psi(\vec{r})$, we can implicitly determine the obtained Hamiltonian $\hat{H}$ by the value $n(\vec{r})$.

The DFT-LSDA calculated electron density of states for a supercell of the Ti_3Sb compound is shown in Fig. 2, *b*. The main DOS peaks are shown by two colors (black and red): the black curve (peaks) corresponds to electrons with the „spin-up“ direction (spin direction coincides with the direction of magnetic material magnetization), and the red one — with the „spin-down“ (spin and magnetization are differently directed).

There are no electrons in the band structure at points of high symmetry M and R for the cubic crystal system of A15 Ti_3Sb in the energy range of -10.0 eV to -6.0 eV (Fig. 2, *a*). This is due to the fact that the Ti_3Sb intermetallide, like metals, has no band gap typical for semiconductors and dielectrics. The energy band near the valence band bottom (near -11.0 eV) is conditioned by *s*-states of Ti and Sb atoms located in the Ti_3Sb lattice.

Ti and Sb atoms in the A15 Ti_3Sb lattice are packed close to each other, that's why each atom touches several other atoms and creates a crystal lattice with a metallic bond. Electrons in such a lattice are delocalized and move freely. Ti_3Sb atoms at the outer level have few electrons (Ti $4s^2$; Sb $5p^3$) as compared to the total number of electrons of outer orbitals.

It is known that metal atoms easily donate outer electrons and turn into ions: $Me - n\bar{e} \rightarrow Me^{n+}$. Then atom electrons connect with ions and convert them into atoms: $Me^{n+} + n\bar{e} \rightarrow Me$. Electrons of each metal atom are divided on the orbitals of surrounding atoms. Due to this, electrons can migrate through the intermetallide crystal lattice from their „parent“ atoms which then receive new electrons. Then electrons again separate from the metal atom and connect to other Me^{n+} ions and so on: $Me - n\bar{e} \leftrightarrow Me$.

In other words, positive ions of Me^{n+} metals in A15 Ti_3Sb are attracted to one another due to a metallic bond and electrons are shared. Therefore, the crystal structure of an intermetallide, like that of a metal, consist of metal cations around which a shared electron cloud moves freely (it pertains to the whole intermetallide „lump“). According to the aforesaid, the conduction band and valence band in Ti_3Sb overlap and form one overlap band. In this case, an electron in Ti_3Sb can freely move in the overlap band, having obtained low energy.

Similar peculiarities of the band electronic structure in intermetallic superconductors with the A15 structure are also observed in other similar materials, e.g., in Ti_3Sb, Ti_3Sn, Ti_3Pb [43], Ta_3Sb, Ti_3Ir [44] and W_3Ta [45].

The DFT (PBE) calculations of the band structure in [43,44,46,47] showed that A15 compounds (space group $Pm\bar{3}n$; № 223) have a non-trivial band and electronic structure. This leads to the formation of topologic surface

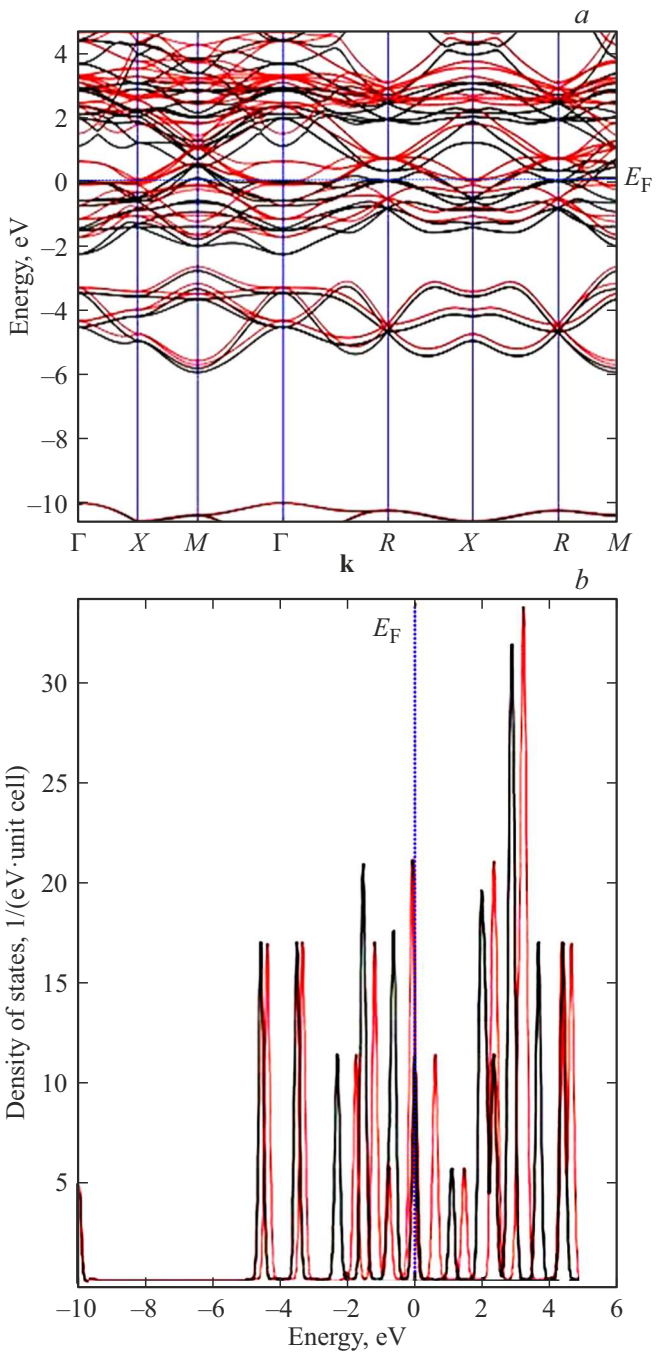

Figure 2. DFT-LSDA calculated band structure (a) and total density of states (DOS) (b) for the model of the $2\times2\times2$ supercell of the A15 Ti_3Sb compound (space group $Pm\bar{3}n$) near the Fermi energy E_F. The Fermi level was found to be equal to $E_F = 0$ eV. The band structure is shown along the highly-symmetrical directions in the first Brillouin zone. The black DOS curve (peaks) corresponds to electrons with the „spin-up" direction, and the red curve — with the „spin-down".

states near the Fermi level. The electronic structure of A15 superconductors (in particular, W_3Ta) was calculated on the basis of DFT-GGA in [45]. It was shown that the arising large own spin Hall effect, which generates spin currents, in W_3Ta and other A15 superconductors can be caused by crystal and band symmetry.

3.1.3. Partial densities of states

The DFT-LSDA calculated partial densities of states (PDOS) for the $2\times2\times2$ supercell of A15 Ti_3Sb are shown in Fig. 3, *a, b, c*. It follows from the PDOS calculation results for A15 Ti_3Sb that there is a spin imbalance in the population of energy levels at the Fermi level for s-, p-, d-states with the spin up and down.

According to PDOS in Ti_3Sb, densities of vacant states of Ti ($3d^24s^2$) and Sb ($4d^{10}5s^25p^3$) electrons with different spins (different spin projections to the quantization axis) are not identical and these electron states have different energies. Such an energy shift leads to the filling of the allowed bands of Ti_3Sb (in particular, by Ti-$3d^2$ and Sb-$3d^1$) electrons with the same specific spin and the formation of a local magnetic moment. In this case, the spin eigen polarization of electrons ($P = (n_\uparrow - n_\downarrow)/(n_\uparrow + n_\downarrow)$) determines the pattern of energy band population with electrons having different spins ($n_\uparrow$ and $n_\downarrow$, where n is electron concentration).

In other words, the value of potential where Ti_3Sb electrons are localized depends on the Coulomb interaction between electrons (E_d), influence of exchange interaction (E_x) and degree of electron spin polarization. It means that the spin-orbital (SO) interaction also makes a contribution to the spin imbalance of population in Ti_3Sb.

The above-mentioned effects of a change of the A15 Ti_3Sb potential may result in the formation of a fine structure of electron energy spectrum and splitting of spectra of Ti and Sb atoms. In this case, the spin imbalance in the population of energy levels and spin-orbital interaction in Ti_3Sb cause the effects of spin polarization (SP) of electron states. Thus, SP effects lead to the modification of the spin structure of A15 Ti_3Sb and splitting of valence electron states of atoms by spin.

Similar results of PDOS in Ti_3Sb have been obtained earlier using ab initio calculations in [44,46]. The DFT-LSDA calculated peaks of partial density of s-, p-, d-states of Ti and Sb atoms agree well with the known data on PDOS in Ti_3Sb [44].

An Sb atom in A15 Ti_3Sb can receive three electrons for attaining the closed shell configuration. After the valence $5p$-orbitals are filled, Sb^{3-} assumes the noble gas configuration. Valence $5p$-orbitals of Sb make a contribution to the band located 3–6 eV below the estimated Fermi level and is separated from the conduction band. The latter mainly consists of Ti $3d$ and $4s$-states and corresponds to relative electronegativity of Ti and Sb. The band formed by valence $5s$-orbitals of Sb is located 10–11.6 eV below the Fermi level. The Fermi level for Ti_3Sb falls on the peaks of the DOS curves, which means that superconductivity is possible in the Ti_3Sb compound.

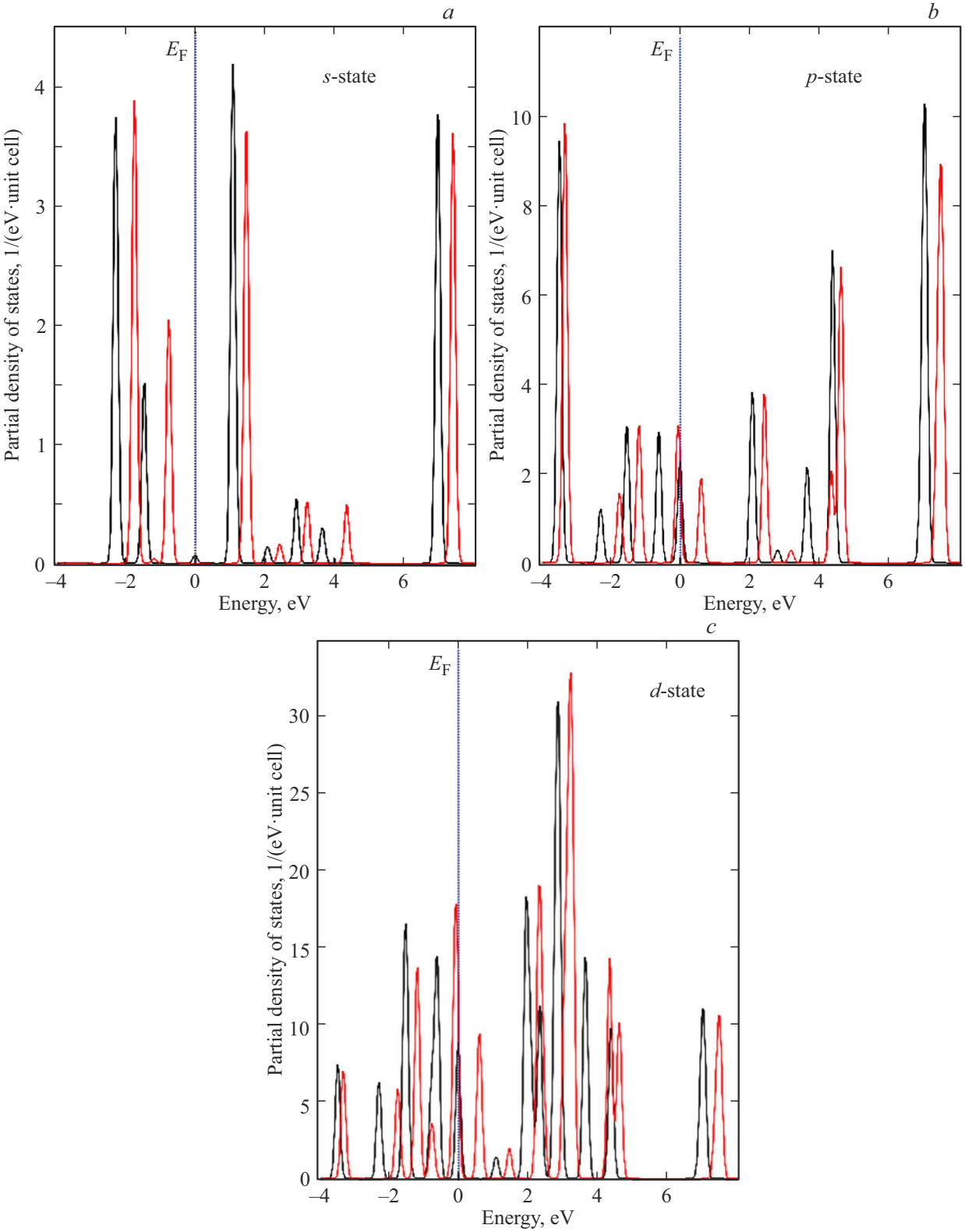

Figure 3. DFT-LSDA calculated partial densities of states (PDOS) for *s*-, *p*-, *d*-orbitals of the $2 \times 2 \times 2$ supercell of A15 Ti_3Sb compound (space group $Pm\bar{3}n$): *a*) *s*-state, *b*) *p*-state, *c*) *d*-state. The Fermi level was found to be equal to $E_F = 0$ eV. The black PDOS curve (peaks) corresponds to electrons with the „spin-up“ direction, and the red PDOS curve — with the „spin-down“.

3.1.4. Magnetic moment

Titanium and antimony atoms in A15 Ti_3Sb are located in different crystal lattice sites. That's why non-equivalent atom positions and symmetry of two site types cause a difference of partial magnetic moments (M_i, μ_B is the Bohr magneton or elementary magnetic moment) of Ti and Sb atoms. It follows from the DOS spectra of the $2 \times 2 \times 2$ supercell of the A15 Ti_3Sb compounds that the main electrons which ensure a magnetic interaction between Ti_3Sb crystal atoms are $3d^2$ are titanium electrons. Since $3d$-shells of Ti are partially occupied, the empty outer electron levels are filled due to hybridization, in particular, $4s^2$- and $5p^3$-electrons of Ti and Sb. Initial configurations of valence Ti and/or Sb electrons can also change due to point defects in the crystal structure of A15 Ti_3Sb.

The full and partial magnetic moments were obtained for geometrically optimized $2 \times 2 \times 2$ supercells based on the A15 Ti_3Sb compound. Exchange integrals in the Hamiltonian are considered in the following form:

$$\hat{H} = -\sum_{i \neq j} J_{ij} S_i S_j,$$

where J_{ij} are parameters of magnetic exchange interaction between atoms i and j, S_i is the full spin of atom i. The magnetic moment of atom i, related to spin S_i, was calculated according to the correlation: $M_i = g\,\mu_B S_i$, where g is the Lande factor (gyromagnetic multiplier).

The relaxed parameter of the A15 Ti_3Sb lattice ($a = 5.217$ Å) agreed well with the experimental A15 Ti_3Sb lattice ($a = 5.2228$ Å [11]). Partial lattice relaxation was performed by shifting titanium atoms, the nearest neighbors of the Sb atom, to distance $\delta r = 0.006$ Å along the cube main diagonal. In this case, the total energy of a partially relaxed lattice was lower ($E = -1387.85$ eV) than the corresponding quantity for a non-relaxed lattice ($E = -1387.83$ eV). This shows that a cubic lattice is distorted insignificantly under geometric relaxation of a lattice cell of A15 Ti_3Sb. That's why the obtained results for magnetic moments do not greatly differ when relaxation is taken into consideration or neglected.

Implantation of Ti or Sb monovacancies in the structure of the Ti_3Sb crystal supercell greatly changes the value of the local magnetic moment. Table 2 gives the DFT-LSDA calculated total magnetic moments and energy of the A15 Ti_3Sb compound containing Ti or Sb vacancies in different Ti_3Sb cell sites ($a = 5.217$ Å). There are no experimental measurements of magnetization for A15 Ti_3Sb. When calculating the magnetic moment, we assumed that this quantity corresponds to the unit cell M_i value, taken relative to the number of magnetic atoms, in particular, Ti in a cell M_{tot}. The local magnetic moment means the total spin density of d-like electrons in the MT-potential approximation. The MT potential is considered to be spherically symmetric around atom cores and constant in the interstitial space.

The value of the local magnetic moment is determined, in particular, by the following interrelated factors. The first factor is related to the overlapping of wave functions of d-states, which change with an increase of the quantity of impurities or increase of the interatomic distance. The second factor is related to levelling of the d-band with an increase of $s-d$ hybridization at a titanium site due to dithe stortion of the potential by the implanted impurity. The locality of $s-d$ hybridization leads to a dependence of impurity impact on distance.

Table 2. DFT-LSDA calculated total magnetic moment (M_{tot}) and total energy (E) of $2 \times 2 \times 2$ supercells based on the A15 Ti_3Sb compound with a cubic crystal system

$2 \times 2 \times 2$ A15 supercell Ti_3Sb	A15 Ti_3Sb (space group $Pm\bar{3}n$; № 223; $a = 5.217$ Å)		
	M_{tot}, μ_B		E, eV
Ti_3Sb	0.08	0.073 [46]	−1387.85
Ti_3Sb with Ti vacancy	0.97		−1205.58
Ti_3Sb with Sb vacancy	1.11		−1232.63

The spin magnetic moment of the d-shell of Ti ions make a considerable contribution to the total magnetic moment of Ti_3Sb. The magnetic moment value increases when a Ti or Sb vacancy forms in $2 \times 2 \times 2$ supercells of Ti_3Sb (Table 2). The DFT-LSDA calculated magnetic moments of atoms of $2 \times 2 \times 2$ supercell based on the A15 Ti_3Sb compound exceed the value for „pure" A15 Ti_3Sb ($M_{tot} = 0.08\,\mu_B$). Our calculation for „pure" A15 Ti_3Sb ($M_{tot} = 0.08\,\mu_B$) agrees with the known value ($M_{tot} = 0.073\,\mu_B$ [46]). The differences in local magnetic moments (difference $\Delta M_{tot} = 0.007\,\mu_B$ is within the error) in the equivalent positions in A15 Ti_3Sb can be explained by the differences in calculation methods and lattice parameter. Magnetic moment in metal alloys often increases with an increase of the lattice parameter. Disordering upon implantation of Ti or Sb vacancies into the supercell results in a change of the magnetic moment of A15 Ti_3Sb.

3.2. Atomic and band structures: $D8_m$ Ti_3Sb (tetragonal crystal system)

DFT-LSDA calculations of the electronic structure of $D8_m$ Ti_3Sb have not been performed previously. Therefore, the determination of the energy band structure of electrons in the $D8_m$ Ti_3Sb crystal is interesting in itself. This is also necessary for a comparative analysis of electronic and magnetic properties of two Ti_3Sb modifications.

3.2.1. Atomic structure

DFT-calculations of $2 \times 2 \times 2$ supercells based on the $D8_m$ Ti_3Sb compound with a tetragonal crystal system

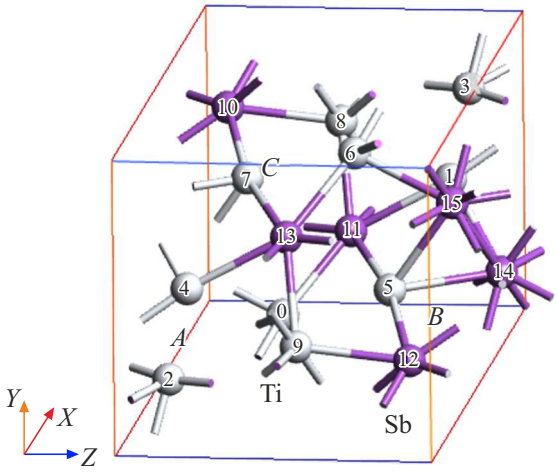

Figure 4. Relaxed atomic structure of a $2 \times 2 \times 2$ supercell of a tetragonal modification of the $D8_m$ Ti_3Sb compound (space group $I4/mcm$). Sb atoms are painted purple, while Ti atoms are gray.

(prototype Cr_5Si_3, space group $I4/mcm$; № 140) were performed. The cell parameters of the Ti_3Sb tetragonal crystal system were relaxed. Crystallographic positions of atoms were chosen as follows: Ti (4b) 0, 1/2, 1/4, Ti (16k) x, y, 0, Sb (4a) 0, 0, 1/4, Sb (8h) x, $x + 1/2$, 0. The optimized cell parameters of the $D8_m$ Ti_3Sb tetragonal crystal system were $a = 10.457$ Å, $c = 5.258$ Å, which agree with the experimental data ($a = 10.465$ Å, $c = 5.2639$ Å [5]). Fig. 4 shows the relaxed atomic structure of the $D8_m$ Ti_3Sb supercell.

3.2.2. Band structure of $D8_m$ Ti_3Sb

The band structure along the crystallographic c-axis of the crystal of a tetragonal modification of a $2 \times 2 \times 2$ supercell of $D8_m$ Ti_3Sb near the Fermi level and total density of states are shown in Fig. 5, *a, b*.

A comparison of the results of the DFT-LSDA calculations shows that the electronic structures of the cubic and tetragonal Ti_3Sb phases are on the whole similar in nature. As distinct from the cubic structure of A15 Ti_3Sb (Fig. 2, *a*), the crystalline potential in the electronic band structure of $D8_m$ Ti_3Sb (Fig. 5, *a*) deviates from the MT-potential approximation due to the dominant impact of „chains“ of Ti sites.

3.2.3. Electronic structure

PDOS for s, p, d-electrons of the $D8_m$ Ti_3Sb structure with the spin up and down shows that this modification is also characterized by the spin imbalance in the population of energy levels, related to spin effects (Fig. 6, *a, b, c*).

A comparison of the DOS spectra for the $D8_m$ Ti_3Sb and A15 Ti_3Sb modifications shows that the DOS profiles of tetragonal crystal system ($D8_m$) across the Fermi level demonstrate a lower metallic behavior. Atoms in A15 Ti_3Sb, as compared to $D8_m$ Ti_3Sb, are located relatively close, and therefore the cubic lattice (A15) has a low mobility. Atoms in such a lattice are strongly bound, and metallic bonds prevent atoms (or the core which is an ion) from changing their positions.

The density of states for both Ti_3Sb modifications at the Fermi level is mainly determined by d-states of titanium and

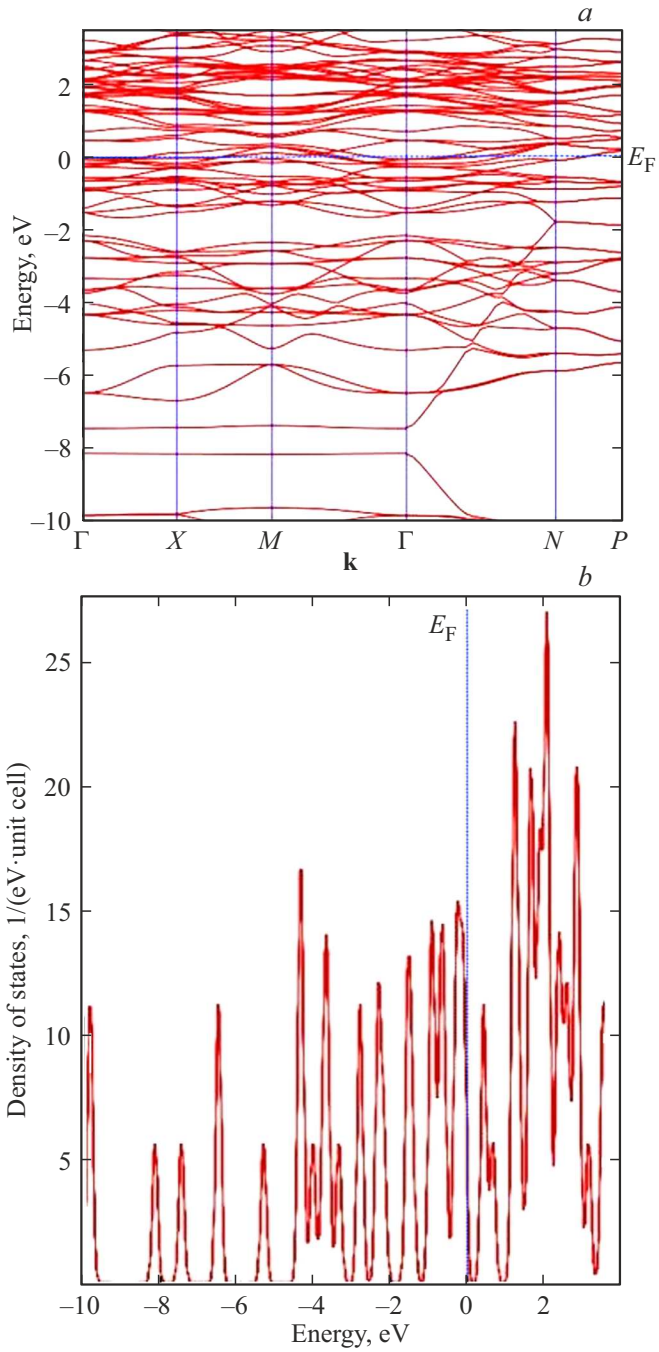

Figure 5. DFT-LSDA calculated band structure (*a*) and total density of states (DOS) of electrons (*b*) for the tetragonal modification of a $2 \times 2 \times 2$ supercell of the $D8_m$ Ti_3Sb compound (space group $I4/mcm$). The Fermi level was found to be equal to $E_F = 0$ eV. The black DOS curve (peaks) corresponds to electrons with the „spin-up“ direction, and the red DOS curve (peaks) — „spin-down“.

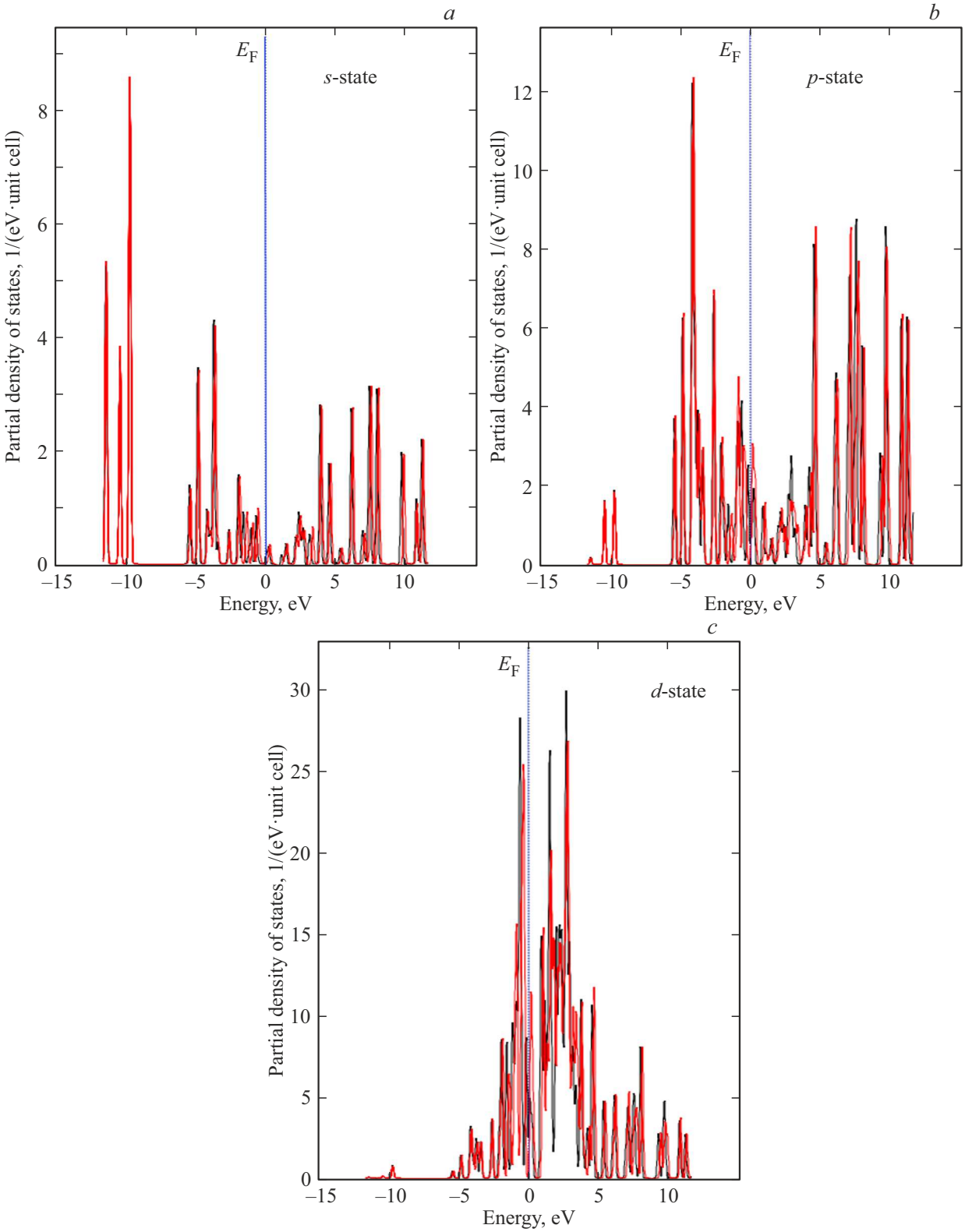

Figure 6. DFT-LSDA calculated partial densities of states (PDOS) of electrons of the $2 \times 2 \times 2$ supercell of $D8_m$ Ti_3Sb compound (space group $I4/mcm$): *a*) *s*-state, *b*) *p*-state, *c*) *d*-state. The Fermi level was found to be equal to $E_F = 0$ eV. The black PDOS curve (peaks) corresponds to electrons with the „spin-up“ direction, and the red PDOS curve (peaks) — with the „spin-down“.

Table 3. DFT-LSDA calculated interatomic distances in $2 \times 2 \times 2$ supercells of the Ti_3Sb compound

Modification Ti_3Sb	Interatomic distance, Å		
	Ti−Sb	Ti−Ti	Sb−Sb
A15 Ti_3Sb	Ti_2-Sb_1 (2.92)	Ti_2-Ti_4 (2.61)	
$D8_m$ Ti_3Sb	$Ti_{10}-Sb_{11}$ (2.80)		$Sb_{14}-Sb_{15}$ (2.63)

Table 4. DFT-LSDA calculated values of magnetic moment (M_{tot}) and total energy (E) of a $2 \times 2 \times 2$ supercell of the $D8_m$ Ti_3Sb modification

$2 \times 2 \times 2$ supercell of $D8_m$ Ti_3Sb	$D8_m$ Ti_3Sb (prototype Cr_5Si_3, space group $I4/mcm$; № 140; $a = 10.457$ Å, $c = 5.258$ Å)		
	M_{tot}, μ_B		E, eV
Ti_3Sb „pure“	0.09	0.079 [47]	−2716.17
Ti_3Sb with Ti vacancy	1.25		−2534.61
Ti_3Sb with Sb vacancy	2.54		−2562.05

p-states of Sb. That's why metallic properties of both Ti_3Sb modifications can be related to the localized hybridization of electrons between a Ti atom and an Sb atom. Hybridization of *pd*-orbitals takes place in the environment of Ti atoms (4b) by four Sb atoms at the distance of 2.8 Å.

3.2.4. Magnetic moment

The calculated atomic distances between Ti and Sb in A15 Ti_3Sb and $D8_m$ Ti_3Sb structures differ from each other. Thus, for instance, the atomic distance between the 2-nd Ti_2 atom and the 1-st Sb_1 atom is 2.92 Å, which is 0.12 Å more than the distance between Ti_{10} and Sb_{11} (Table 3).

It has been established that magnetic moment $D8_m$ Ti_3Sb changes depending on distance between the Ti transition metal and the Sb semimetal, as well as between Ti−Ti, Sb−Sb atoms. The results of the DFT-LSDA calculations of magnetic moments for the $D8_m$ Ti_3Sb compounds are given in Table 4.

Local magnetic moments in the $D8_m$ Ti_3Sb compound with a Ti (or Sb) vacancy differ from each other. The magnetic moment for $D8_m$ Ti_3Sb is $0.09\,\mu_B$, which is close to the value of $0.079\,\mu_B$ previously obtained in [47]. This value is considerably smaller than the magnetic moment of $1.25\,\mu_B$ for $D8_m$ Ti_3Sb which contains a Ti vacancy, and $2.54\,\mu_B$ for $D8_m$ Ti_3Sb containing an Sb vacancy.

Lithium doping and formation of Ti or Sb vacancies in $2 \times 2 \times 2$ supercells of the $D8_m$ Ti_3Sb modification change the interatomic distance in $D8_m$ Ti_3Sb. The forming local magnetic moments in the Ti_3Sb lattice near Ti or Sb vacancies change accordingly.

A comparison of the results of the DFT-LSDA calculations of crystalline, magnetic and band parameters of the two Ti_3Sb modifications shows the presence of two systems of crystallographically non-equivalent sites (sublattices) in the crystal lattice, occupied by magnetic Ti and semimetallic Sb atoms. The following takes place inside of each of Ti_3Sb sublattices and between them: competing interactions and exchange between Ti and Sb atoms (ions) of different coordination, which ensures the mutual position of spins in the crystal.

3.3. Formation enthalpy and cohesion energy

It is known that the standard heat (or enthalpy) of formation ($\Delta_f H^0_{299.15}$) is the heat of the reaction of formation of 1 mole of a complex substance from elements. It is assumed in this case that its constituent elements are in a stable state of matter under the standard conditions. It means that the compound formation enthalpy, which is related to the internal system energy, allows for estimating the thermodynamic capacity of formation of 1 mole of a complex substance from standard elements. The value of $\Delta_f H_0$ for a supercell of the Ti_3Sb compound at $T = 0$ K was calculated by the DFT-LSDA method as a difference of the total energy between the Ti_3Sb compound and its Ti and Sb components in relation to the stoichiometric composition of Ti_3Sb:

$$\Delta_f H_0(Ti_3Sb) = [E_{total}(Ti_3Sb) - n \cdot E_{solid}(Ti) - m \cdot E_{solid}(Sb)]/4, \quad (1)$$

where $E_{total}(Ti_3Sb)$ is total energy of the Ti_3Sb compound; $n = 3$, $m = 1$ — number of atoms of the Ti and Sb element,

Table 5. DFT-LSDA calculated lattice constants (calculated/experiment — cal/exp), formation enthalpy and cohesion energy of Ti_3Sb modifications

Ti_3Sb	Space group	a, Å (cal/exp)	c, Å (cal/exp)	$-\Delta_f H_0$, eV/atom	$-\Delta E_c$, eV/atom
A15	$Pm\bar{3}n$	5.217/5.2228 [11]	5.217/5.2228 [11]	0.44 0.379 [46]	6.27
$D8_m$	$I4/mcm$	10.457/10.465 [5]	5.258/5.2639 [5]	0.37i 0.325 [47]	5.34

respectively, in a unit cell; $E_{solid}(Ti)$ and $E_{solid}(Sb)$ — energy per atom of the Ti and Sb element, respectively, in the crystal structure in the solid state.

A similar method was used to calculate the cohesion energy (bond between identical molecules (atoms, ions) inside a body) ΔE_c, which characterizes the structural strength of the Ti_3Sb compound. The atom cohesion energy in Ti_3Sb was determined as the work for the decomposition of a Ti_3Sb compound crystal into separate free atoms

$$\Delta E_c(Ti_3Sb) = [E_{total}(Ti_3Sb) - 3E_{atom}(Ti) - E_{atom}(Sb)]/4, \quad (2)$$

where — $E_{atom}(Ti)$ and $E_{atom}(Sb)$ is the energy per Ti and Sb atom in the isolated state, respectively.

The results of calculations of formation enthalpy $\Delta_f H_0$, atom cohesion energy ΔE_c and lattice constants for Ti_3Sb are given in Table 5.

A comparison of the structural and thermodynamic data for Ti_3Sb [46,47] and our calculation results shows that they mainly agree with each other. The scatter in the DFT-LSDA calculated values of Ti_3Sb crystal formation enthalpy from the known values of $-\Delta_f H_0$ can be related, in particular, to the different parameters of the lattices of the Ti_3Sb modifications used in the calculations (Table 5).

3.4. Li-doped A15 Ti_3Sb compound

Large-scale use of lithium-ion storage batteries (LISB) on the basis of a carbon anode is limited by their performance indicators (low charging rate, narrow interval of operating temperatures and insufficient safety). LISB modernization is related to the development of new electrode materials capable of ensuring the required energy and performance indicators. That's why a topical task is the search of LISB electrode materials capable of maintaining structure stability under repeated implantation/removal of Li^+.

A promising substitute for the carbon anode can be titanium compounds (e.g., TiO_2 and $Li_4Ti_5O_{12}$), which have a potential of about 1.5−1.8 V in relation to the lithium reference electrode and an increase structure stability under cycling. However, a large band gap (3.0−3.2 eV) and a low electrical conductivity ($\sim$ 10−12 S/cm) of TiO_2 hinder its use as a LISB anode. Moreover, it is known that the crystal lattice of titanium dioxide considerably deforms ($\sim$ 3%) after implantation/removal of lithium ions into TiO_2. Considering the aforesaid, synthesis of intermetallic Ti_3Sb, doped with lithium ions, in the nanostructured form seems to be an efficient approach for the making of anode materials for metal-ion storage batteries. The formation of ternary intermetallides in the Ti−Sb−Li system was not reported in any publications.

The Ti−Sb−Li system has been studied based on the data about phase equilibriums of Ti−Sb binary systems [4–6], Ti−Li [34], Sb−Li [35–39] and thermodynamic properties of binary compounds in them. The structural stability of binary compound and stability of conodes between them in the Ti−Sb−Li system was determined by the thermodynamic method. DFT calculations of enthalpy of formation of Ti−Sb−Li alloys and Ti_3Sb-based compounds were performed considering the procedure described in [48].

The reaction of lithium implantation into the initial Ti_aSb_b lattice can be schematically represented as

$$Ti_aSb_b + xLi^+ + x\bar{e} \leftrightarrow Ti_aSb_bLi_c.$$

In this case, the value $\Delta_f H_0$ for a 64 atom supercell of a sample consisting of $Ti_aSb_bLi_c$ was calculated at $T = 0$ K using the formula

$$\Delta_f H_0(Ti_aSb_bLi_c) = [\Delta E_{total}(Ti_3Sb_bLi_c)] - a[\Delta E_{total}(Ti)/j] - b[\Delta E_{total}(Sb)/k] - c[\Delta E_{total}(Li)/l]/a + b + c, \quad (3)$$

where a, b, c, d is the number of atoms of each type in the crystal lattice of the compound used in calculations; j, k, l — number of atoms in the crystal lattice of Ti, Sb and Li, respectively, used in calculations; E_{tot} — total compound energy in eV.

The DFT calculated formation enthalpy for Ti_3Sb was −0.44 eV/atom (Table 5), for Li_3Sb −0.84 eV/atom, for $Ti_3Sb_{0.9792}Li_{0.0208}$ (−0.43 eV/atom), for $Ti_3Sb_{0.9792}Li_{0.0208}$ (−0.43 eV/atom), for $Ti_{2.9375}SbLi_{0.0625}$ (−0.42 eV/atom).

A Ti_3Sb-based supercell was modelled with account of lithium doping of its structure. Filling of Ti_3Sb padding lattice vacancy in the position of the 4*d*-state of Ti by Li atom doping is energetically profitable up to compounds in the homogeneity range (< 1 mole%) on the basis of Ti_3Sb. A decrease of $Ti_{3-x}Sb_yLi_{x-y}$ formation enthalpy is observed in the concentration dependence of Ti_3Sb−Li when Ti in the Ti_3Sb lattice is substituted by a lithium atom.

Using the data on the systems of Ti−Sb [4–6], Ti−Li [34], Sb−Li [35–39] and based on DFT-calculation, we have plotted an isothermal cross-section of the $T - x$ diagram for the Ti−Sb−Li system at $T = 298$ K (Fig. 7). The isothermal section of the diagram shows the phase and structural composition for all concentrations of Ti−Sb−Li ternary alloys at 298 K. It can be seen that the solubility of

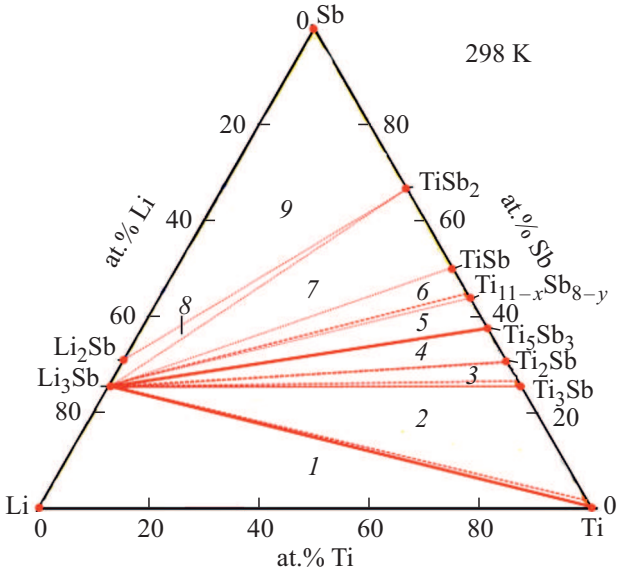

Figure 7. Isothermal section of the Ti–Sb–Li system at 298 K: *1* — $Li_3Sb + Li + Sb$, *2* — $Li_3Sb + Ti + Ti_3Sb$, *3* — $Ti_3Sb + Li_3Sb + Li_2Sb$, *4* — $Ti_5Sb_3 + Li_3Sb + Li_2Sb$, *5* — $Ti_5Sb_3 + Li_3Sb + Ti_{11-x}Sb_{8-y}$, *6* — $TiSb + Li_3Sb + Ti_{11-x}Sb_{8-y}$, *7* — $TiSb + Li_3Sb + TiSb_2$, *8* — $Li_2Sb + Li_3Sb + TiSb_2$, *9* — $Li_2Sb + Sb + TiSb_2$.

components based on binary compounds in the solid state is insignificant.

3.4.1. Atomic structure of A15 Ti_3Sb–Li

The structure of the A15 Ti_3Sb–Li supercell was modelled by Ti_3Sb doping with Li atoms, where Li atoms substitute Ti and/or Sb atoms separately. Lithium doping was performed with a change of lithium concentration in Ti_3Sb–Li. A Ti_3Sb supercell containing 64 atoms was doped with lithium in the concentration of 6.25 at.% Li for the substitution of Ti atoms and 2 at.% Li for the substitution of Sb atoms, respectively. The substitution of Ti and/or Sb components in the Ti_3Sb compound by Li atoms in a supercell results in compounds $Ti_3Sb_{0.9792}Li_{0.0208}$ and $Ti_{2.9375}SbLi_{0.0625}$. The atomic structure of the said A15 Ti_3Sb–Li supercell containing 64 atoms is shown in Fig. 8. The DFT calculations show that the substitution of Ti and/or Sb atoms in the Ti_3Sb compound separately by Li atoms does not affect the atomic positions of Ti and/or Sb in the lattice. Li-doping with the substitution of Ti or Sb atoms in the Ti_3Sb lattice in both cases ($Ti_{3-x}SbLi_x$ and $Ti_3Sb_{1-x}Li_x$) reduces the crystal lattice parameters. Thus, for instance, the DFT calculated lattice parameter $Ti_3Sb_{0.9792}Li_{0.0208}$ (structural type Cr_3Si, space group $Pm\bar{3}n$) is $a = 5.207$ Å, $V = 141.10$ Å^3, which is smaller than the lattice parameter of „pure“ A15 Ti_3Sb: $a = 5.217$ Å, $V = 141.77$ Å^3 (Table 2).

The DFT-LDA calculation for A15 Ti_3Sb and Ti_3Ir compounds (type Cr_3Si) has determined the maximum number of atoms of hydrogen implanted in the lattice of these intermetallic compounds [44]. It has been shown that hydrogen atoms in Ti_3SbH_n and Ti_3IrH_n are attracted to tetrahedral interstices [Ti_4] more than to other positions. The nature of the metal–hydrogen and metalloid–hydrogen bond, as well as the influence of hydrogen implantation on the metal–metal bond of Ti–Sb or Ti–Ir, as well as metal–metalloid of Ti–Ti_3Sb determine the maximum content of hydrogen atom content in Ti_3Sb and Ti_3Ir. In this case, the Ti–Ti bond is partially substituted by the Ti–H bond, and this effect has an impact on their superconducting behavior.

3.4.2. Magnetic moment of A15 Ti_3Sb–Li

We have performed DFT-LSDA-calculations of the magnetic moment of a supercell of the A15 Ti_3Sb–Li structure with Ti or Sb substitution by a Li atom. Given the small difference in the ionic radius values, a partial substitution of Ti^{3+} ions (0.067 nm) or Sb^{5+} (0.060 nm) ions by Li^+ (0.076 nm) does not greatly change the cubic lattice parameter. Such a Li-substitution corresponds to the formation

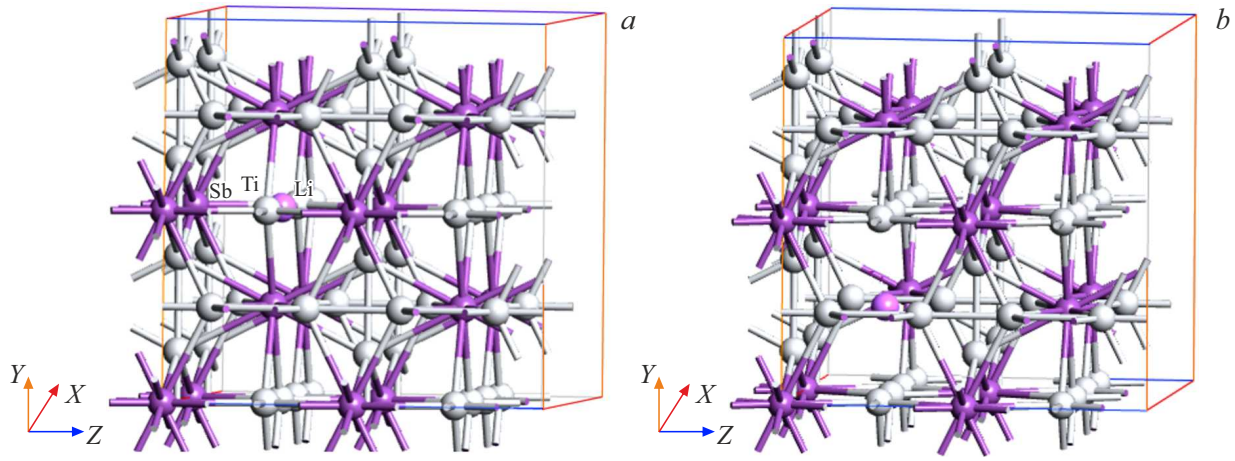

Figure 8. Atomic structure of Li-doped A15 Ti_3Sb compound (space group $Pm\bar{3}n$). Supercells: *a*) $Ti_{2.9375}SbLi_{0.0625}$, *b*) $Ti_3Sb_{0.9792}Li_{0.0208}$.

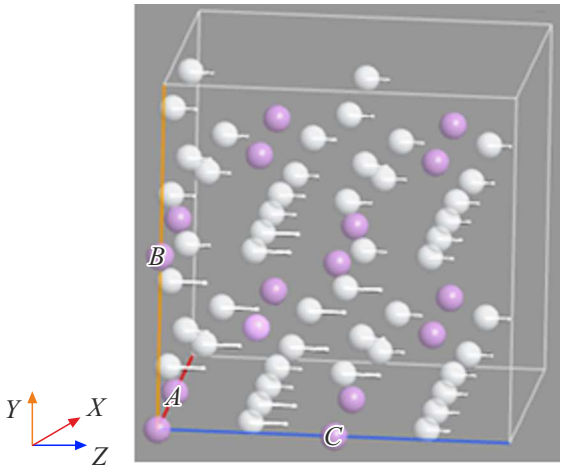

Figure 9. Direction of local magnetic moment of atoms in a 64 atom A15 $Ti_3Sb_{0.9792}Li_{0.0208}$ supercell (space group $Pm\bar{3}\,n$).

of local lithium clusters in the A15 Ti_3Sb–Li lattice. The calculated total magnetic moments for $Ti_3Sb_{0.9792}Li_{0.0208}$ and $Ti_{2.9375}SbLi_{0.0625}$ per formula unit are given in Table 6.

An increase of Li dopant concentration in $Ti_{3-x}SbLi_x$ and $Ti_3Sb_{1-x}Li_x$ results in an increase of magnetic moment and absolute value of total supercell energy (Table 6), which confirms the actual implantation of Li^+ into the

Table 6. DFT-LSDA calculated total magnetic moment (M_{tot}) and total energy (E) of supercells based on the A15 Ti_3Sb compound with a cubic crystal system

Supercell based on A15 Ti_3Sb	A15 Ti_3Sb (space group $Pm\bar{3}n$; № 223; $a = 5.217$ Å)		
	M_{tot}, μ_B		E, eV
Ti_3Sb	0.08	0.073 [46]	−1387.85
$Ti_{2.9375}SbLi_{0.0625}$	2.11		−10933.39
$Ti_3Sb_{0.9792}Li_{0.0208}$	3.53		−10961.04

A15 Ti_3Sb lattice with the formation of $Ti_{3-x}SbLi_x$ and $Ti_3Sb_{1-x}Li_x$ solid solution. In this case, the volume of the unit cell ($Ti_{3-x}SbLi_x$ and $Ti_3Sb_{1-x}Li_x$), which changes insignificantly, correlates with the Li/Ti and Li/Sb atomic ratio. A small increase of the volume of the A15 Ti_3Sb unit cell due to lithium implementation can reduce the crystal lattice structural stresses caused by the implantation/removal of Li^+ ions. This follows indirectly from the calculated total energies of the equilibrium configurations based on A15 Ti_3Sb (Table 6). Implementation of lithium atoms into the A15 Ti_3Sb structure considerably increases the value of local magnetic moment. This can be related to an increased

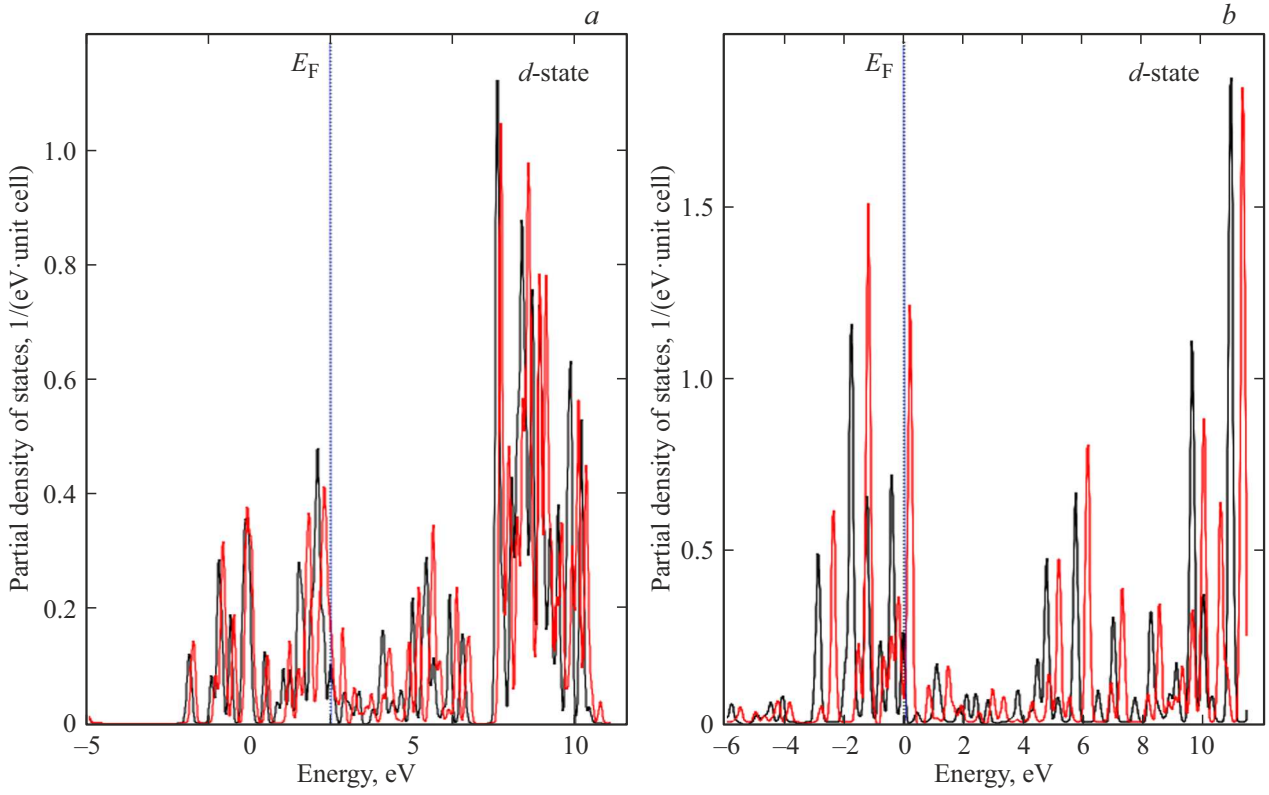

Figure 10. DFT-LSDA calculated partial densities of states (PDOS d-state) of electrons of supercells based on A15 Ti_3Sb–Li (space group $Pm\bar{3}n$): *a*) $Ti_{2.9375}SbLi_{0.0625}$, *b*) $Ti_3Sb_{0.9792}Li_{0.0208}$. The Fermi level was found to be equal to 0 eV. The black PDOS curve (peaks) corresponds to electrons with the „spin-up“ direction, and the red PDOS curve (peaks) — with the „spin-down“.

speed of electron rotation and motion in atoms of the Ti_3Sb lattice due to the contribution of mobile monovalent lithium ions to the magnetic structure and a high spin polarization of conduction electrons.

Fig. 9 shows the magnetic field direction for Ti atoms in an A15 $Ti_3Sb_{0.9792}Li_{0.0208}$ supercell. The DFT-LSDA calculated local magnetic moments of Ti atoms, which surround the doped Li atoms in A15 $Ti_{2.9375}SbLi_{0.0625}$ and $Ti_3Sb_{0.9792}Li_{0.0208}$ structures, were considerably lower than the total magnetic moment values.

The local (total) magnetic moment of Ti atoms ($1.04\,\mu_B$), which surround Li atoms in the structure, e.g., $Ti_{2.9375}SbLi_{0.0625}$, is: $0.76\,\mu_B$ for the 7-th Ti atom and $0.72\,\mu_B$ for the 55-th Ti atom respectively, which is considerably smaller than M_{tot} $Ti_{2.9375}SbLi_{0.0625}$ (Table 6)

Thus, the difference of local magnetic moments of different modifications (A15 and $D8_m$) on the basis of Ti_3Sb and Ti_3Sb-Li can be related to the correlation of competing intra- and inter-sublattice exchange interactions. Moreover, translation symmetry (i.e. periodicity in atom or ion arrangement) and equivalence of sites in sublattices of the cubic and tetragonal Ti_3Sb structure differ from each other. All sites in a cubic A15 Ti_3Sb sublattice with a „stronger bond between particles" are occupied by identical atoms (ions), while particles in the tetragonal $D8_m$ Ti_3Sb phase are located in a „distorted" sublattice. The A15 and $D8_m$ modifications in the $Ti_{3-x}SbLi_x$ and $Ti_3Sb_{1-x}Li_x$ structures also differ by spin configurations and level of Ti and/or Sb substitution by lithium in crystal sublattices.

3.4.3. Electronic structure of A15 Ti_3Sb-Li

The DFT-LSDA calculated intermetallic electronic structures on the basis of A15 Ti_3Sb-Li (in particular, $Ti_{2.9375}SbLi_{0.0625}$ and $Ti_3Sb_{0.9792}Li_{0.0208}$) for *d*-orbitals, taking into account the spin-polarization, are shown in Fig. 10. It follows from the analysis of the PDOS spectra (*d*-state) that doped Li atoms affect electronic structures on the basis of A15 Ti_3Sb-Li. Thereat, the Ti−Ti bond in the crystal lattice structure is substituted by a Ti−Li bond. Such an effect of Li-doping can affect the superconducting behavior of the A15 Ti_3Sb structure due to a change of the size factor, packing density and electron concentration.

4. Conclusion

The calculations within the framework of the density functional theory (DFT) in the local spin density approximation (LSDA) of the band structure, magnetic moment, lattice constants, formation enthalpy and cohesion energy of supercells containing lithium and/or own vacancies of two Ti_3Sb modifications (cubic crystal system, structural type A15, prototype Cr_3Si, space group $Pm\bar{3}n$; № 223; $a = 5.217$ Å); tetragonal crystal system, structural type $D8_m$, (prototype Cr_5Si_3, space group $I4/mcm$; № 140; $a = 10.457$ Å, $c = 5.258$ Å) have shown the following.

The DFT-LSDA calculated total electron energies and densities of states (DOS) and band structures of supercells based on A15 Ti_3Sb and $D8_m$ Ti_3Sb modifications, incl. Li-doped structures, have shown energy stability of these two modifications with a metallic bond. The electronic structure and Fermi surfaces of both modifications (A15 and $D8_m$) of Ti_3Sb are similar to each other. A metallic bond forms in both structures due to valence electrons which optimize the heteroatomic Ti−Sb bonds. The characteristics of electron density distribution indicate that „metallicity" in samples based on the A15 Ti_3Sb modification is greater than in $D8_m$ Ti_3Sb.

The DFT-LSDA calculated magnetic moment depends both on the modifications' structure and on atomic distances (Ti−Sb, Ti−Ti, Sb−Sb) in two $2 \times 2 \times 2$ supercells of the Ti_3Sb modifications. Magnetic moment A15 Ti_3Sb (total local magnetic moment $M_{tot} = 0.08\,\mu_B$) is smaller as compared to magnetic moment $D8_m$ Ti_3Sb (total magnetic moment $0.09\,\mu_B$). Magnetic moments of the A15 and $D8_m$ Ti_3Sb modifications differ if the structure contains different own Ti or Sb vacancies. In particular, it is $0.97\,\mu_B$ in A15 Ti_3Sb (Ti−Sb 2.92 Å) if a Ti vacancy is present, and $1.11\,\mu_B$ if an Sb vacancy is present. Similarly, the following values of M_{tot} have been obtained for the $D8_m$ Ti_3Sb modification (Ti−Sb 2.80 Å): $1.25\,\mu_B$ when a Ti vacancy is present and $2.54\,\mu_B$ when an Sb vacancy is present.

We have DFT-LSDA calculated the lattice constants (A15 Ti_3Sb, $a = 5.217$ Å; $a = 10.457$, $c = 5.258$ Å) and formation enthalpy (A15 Ti_3Sb, $\Delta_f H_0 = -0.44$ eV/atom; $D8_m$ Ti_3Sb, $\Delta_f H_0 = -0.37$ eV/atom) of Ti_3Sb modifications, which agree well with the known data. Li-doping reduces the absolute value of $\Delta_f H_0$ (e.g., for $Ti_3Sb_{0.9792}Li_{0.0208}$ (−0.43 eV/atom), for $Ti_3Sb_{0.9792}Li_{0.0208}$ (−0.43 eV/atom), for $Ti_{2.9375}SbLi_{0.0625}$ (−0.42 eV/atom)). The calculated formation enthalpy of Ti_xSb_y binary compounds (Ti_3Sb was −0.44 eV/atom) and Li_xSb_y (Li_3Sb −0.84 eV/atom) was used to plot an isothermal cross-section (298 K) of a ternary $T-x-y$ phase diagram of Ti−Sb−Li, from which it follows that the solubility of Ti_3Sb-based lithium is insignificant (< 1 at.%).

Li atoms affect the electronic structures of supercells on the basis of A15 Ti_3Sb, and the DOS spectra show that the Ti−Ti bond is partially substituted by a more metallic Ti−Li bond. This effect can affect the superconducting behavior of Ti_3Sb. The value of magnetic moment A15 Ti_3Sb-Li in case of Li-doping of Ti_3Sb increases due to a contribution made by a bond between Ti−Li atoms to the magnetic sublattices which contain Li atoms. The value of magnetic moment increases with an increase of lithium concentration. The total magnetic moment for supercells, e.g., $Ti_3Sb_{0.9792}Li_{0.0208}$ was $2.11\,\mu_B$, and $3.53\,\mu_B$ for $Ti_{2.9375}SbLi_{0.0625}$ per formula unit, respectively.

Acknowledgments

The work has been partially funded by the Science Development Foundation with the President of the Republic

of Azerbaijan (EIF) (grant No. EIF-BGM-4-RFTF-1/2017) and the Russian Foundation for Basic Research (RFBR) (project No. Az_a2018).

Conflict of interest

The authors declare that they have no conflict of interest.

References

[1] W. Steurer, J. Dshemuchadse. Intermetallics: Structures, Properties, and Statistics. Oxford University Press (2016). 592 p. ISBN-13: 9780198714552
[2] M. Mandal, K.P. Sajilesh, R.R. Chowdhury, D. Singh, P.K. Biswas, A.D. Hillier, R.P. Singh. Phys. Rev. B. **103**, 054501 (2021). https://doi.org/10.1103/PhysRevB.103.054501
[3] M. Kim, C. Wang, K. Ho. Phys. Rev. B **99**, 224506 (2019). https://doi.org/ 10.1103/PhysRevB.99.224506
[4] J.L. Murray. Phase Diagrams of Binary Titanium Alloys. ASM International, Metals Park, Ohio(1987). P. 282–284. ISBN-13: 9780871702487
[5] A. Kjekshus, F. Grønvold, J. Thorbjørnsen. Acta Chem. Scand. **16**, 1493 (1962). https://doi.org/10.3891/acta.chem.scand.16-1493.
[6] A. Tavassoli, A. Grytsiv, F. Failamani, G. Rogl, S. Puchegger, H. Müller, P. Broz, F. Zelenka, D. Macciò, A. Saccone, G. Giester, E. Bauer, M. Zehetbauer, P. Rogl. Intermetallics **94**, 119 (2018). https://doi.org/10.1016/j.intermet.2017.12.014
[7] S. Bobev, H. Kleinke. Chem. Mater. **15**, 3523 (2003). https://doi.org/10.1021/cm034328d
[8] M. Armbrüster, W. Schnelle, U. Schwarz, Y. Grin. Inorg. Chem. **46**, 6319 (2007). https://doi.org/10.1021/ic070284p
[9] J. Emsley. The Elements. 2nd ed. Clarendon Press, Oxford (1991). ISBN-13: 978-0198555681
[10] G. Chandra, S. Ramakrishnan, A.K. Nigam. J. Phys. F **16**, 209 (1986). https://doi.org/10.1088/0305-4608/16/2/010
[11] S. Ramakrishnan, G. Chandra. Phys. Lett. **100**, 44 (1984). https://doi.org/10.1016/0375-9601(84)90640-6
[12] J.W. Kaiser, M.G. Haase, W. Jeitschko. Z. Anorg. Allg. Chem. **627**, 2369 (2001). https://doi.org/10.1002/1521-3749(200110)627:103.0
[13] S. Derakhshan, A. Assoud, K.M. Kleinke, E. Dashjav, X. Qiu, S.J.L. Billinge, H. Kleinke. J. Am. Chem. Soc. **126**, 8295 (2004). https://doi.org/10.1021/ja048262e
[14] E. Dashjav, H. Kleinke. **176**, 329 (2003). https://doi.org/10.1016/s0022-4596(03)00214-7
[15] M.T. Sougrati, J. Fullenwarth, A. Debenedetti, B. Fraisse, J.C. Jumas, L. Monconduit. J. Mater. Chem. **21**, 10069 (2011). https://doi.org/10.1039/c1jm10710k
[16] C. Marino, M.T. Sougrati, B. Gerke, R. Pottgen, H. Huo, M. Menetrier, C.P. Grey, L. Monconduit. Chem. Mater. **24**, 4735 (2012). https://doi.org/10.1021/cm303086j
[17] H.A. Wilhelm, C. Marino, A. Darwiche, L. Monconduit, B. Lestriez. Electrochem. Commun. **24**, 89 (2012). https://doi.org/10.1016/j.elecom.2012.08.023
[18] W. Zhang, F. Ghamouss, A. Darwiche, L. Monconduit, D. Lemordant, R. Dedryvere, H. Martinez. J. Power Sour. **268**, 645 (2014). https://doi.org/10.1016/j.jpowsour.2014.06.041
[19] H.A. Wilhelm, C. Marino, A. Darwiche, P. Soudan, M. Morcrette, L. Monconduit, B. Lestriez. J. Power Sour. **274**, 496 (2015). http://dx.doi.org/10.1016/j.jpowsour.2014.10.051
[20] W. Zhang, F. Ghamouss, A. Mery, D. Lemordant, R. Dedryvere, L. Monconduit, H. Martinez. Electrochim. Acta. **170**, 72 (2015). https://doi.org/10.1016/j.electacta.2015.04.009
[21] A. Tavassoli, A. Grytsiv, G. Rogl, V.V. Romaka, H. Michor, M. Reissner, E.B.M. Zehetbauer, P. Rogl. Dalton Trans. **47**, 879 (2018). https://doi.org/10.1039/c7dt03787b.
[22] G.A. Melnyk, W. Tremel. J. Alloys Compd. **349**, 164 (2003). https://doi.org/10.1016/s0925-8388(02)00921-0.
[23] H. Kleinke. Can. J. Chem. **79**, 1338 (2001). https://doi.org/10.1139/cjc-79-9-1338
[24] A.Y. Kozlov, V.V. Pavlyuk. Intermetallics **11**, 237 (2003). https://doi.org/10.1016/s0966-9795(02)00232-7
[25] A. Tkachuk, Yu. Gorelenko, Yu. Stadnyk, B. Padlyak, A. Jankowska-Frydel, O. Bodak, V. Sechovsky. J. Alloys Compd. **319**, 74 (2001). https://doi.org/1016/s0925-8388(01)00915-x
[26] P. Berger, C. Schmetterer, H. Effenberger, H. Flandorfer. J. Alloys Compd. **879**, 160272 (2021). https://doi.org/10.1016/j.jallcom.2021.160272
[27] J. Tobola, J. Pierre. J. Alloys Compd. **296**, 243 (2000). https://doi.org/10.1016/S0925-8388(99)00549-6
[28] V.V. Romaka, P. Rogl, L. Romaka, Yu Stadnyk, N. Melnychenko, A. Grytsiv, M. Falmbigl, N. Skryabina. J. Solid State Chem. **197**, 103 (2013). https://doi.org/10.1016/j.jssc.2012.08.023
[29] O. Senchuk, Y. Tokaychuk, R. Serkiz, P. Demchenko, R. Gladyshevskii. Chem. Met. Alloys. **10**, 76 (2017).
[30] C. Colinet, J.-C. Metal. Mater. Min., **13**, 75 (2016). http://dx.doi.org/10.4322/2176-1523.1077
[31] H. Bie, S.H.D. Moore, D.G. Piercey, A.V. Tkachuk, O.Y. Zelinska, A. Mar. J. Solid State Chem. **180**, 2216 (8) (2007). https://doi.org/10.1016/j.jssc.2007.05.030
[32] A.Y. Kozlov, V.V. Pavlyuk. J. Alloys Compd. **367**, 76 (2004). http://dx.doi.org/10.1016/j.jallcom.2003.08.015
[33] R. Kainuma, R. Umino, X. Xu, K. Han, T. Omori. J. Phase Equilib. Diffus. **41**, 116-112 (2020). https://doi.org/10.1007/s11669-020-00784-7
[34] C. W. Bale. Bull. Alloy Phase Diagrams **10**, 135 (1989). https://doi.org/10.1007/bf02881424
[35] A. Beutl, D. Cupid, H. Flandorfer. J. Alloys Compd. **695**, 1052 (2016). https://doi.org/10.1016/j.jallcom.2016.10.230
[36] D. Li, A. Beutl, H. Flandorfer, D.M. Cupid. J. Alloys Compd. **701**, 186 (2017). https://doi.org/10.1016/j.jallcom.2016.12.399
[37] M.M. Kane, J.M. Newhouse, D.R. Sadoway. J. Electrochem. Soc. **162**, A421 (2015). http://hdl.handle.net/1721.1/102197
[38] J. Sangster, A.D. Pelton. J. Phase Equilib. **14**, 514 (1993). https://doi.org/10.1007/bf02671973.
[39] S. Terlicka, A. Dębski, P.J. Alloys Compd. **673**, 272 (2016). https://doi.org/10.1016/j.jallcom.2016.02.235
[40] M.M. Asadov, S.N. Mustafaeva, S.S. Guseinova, V.F. Lukichev. Phys. Solid State. **63**, 797 (2021). https://doi.org/10.1134/S1063783421050036
[41] M.M. Asadov, S.N. Mustafaeva, S.S. Guseinova, V.F. Lukichev. Phys. Solid State. **62**, 2224 (2020). https://doi.org/10.1134/S1063783420110037
[42] M.M. Asadov, S.S. Guseinova, V.F. Lukichev. Russ. Microelectron. **49**, 314 (2020). https://doi.org/10.1134/S1063739720050030
[43] M. Kim, C.-Z. Wang, K.-M. Ho. Phys. Rev. B 99, 224506(2019). https://doi.org/110.1103/PhysRevB.99.224506
[44] G.J. Miller, R.S. Dissanayaka Mudiyanselage, W. Xie. Z. Naturforsch. B **76**, 819 (2021). https://doi.org/110.1515/znb-2021-0137

[45] E. Derunova, Y. Sun, C. Felser, S.S.P. Parkin, B. Yan, M.N. Ali. Science Adv., **4**, eaav8575. (2019). https://doi.org/10.1126/sciadv.aav8575
[46] https://materialsproject.org/materials/mp-1412/. https://doi.org/10.17188/1190175
[47] https://materialsproject.org/materials/mp-569837/. https://doi.org/10.17188/1275289
[48] M.M. Asadov, E.S. Kuli-zade. J. Alloys Compd. **842**, 155632 (2020)https://doi.org/10.1016/j.jallcom.2020.155632